10-1-2020

A Fictitious Points One-Step MPS-MFS Technique

Xiaomin Zhu
University of Electronic Science and Technology of China

Fangfang Dou
University of Electronic Science and Technology of China

Andreas Karageorghis
University of Cyprus

C. S. Chen
University of Southern Mississippi

A fictitious points one–step MPS–MFS technique

Xiaomin Zhu[*], Fangfang Dou[*] [†], Andreas Karageorghis[‡], C. S. Chen[*] [§]

Abstract

The method of fundamental solutions (MFS) is a simple and efficient numerical technique for solving certain homogenous partial differential equations (PDEs) which can be extended to solving inhomogeneous equations through the method of particular solutions (MPS). In this paper, radial basis functions (RBFs) are considered as the basis functions for the construction of a particular solution of the inhomogeneous equation. A hybrid method coupling these two methods using both fundamental solutions and RBFs as basis functions has been effective for solving a large class of PDEs. In this paper, we propose an improved fictitious points method in which the centres of the RBFs are distributed inside and outside the physical domain of the problem and which considerably improves the performance of the MPS–MFS. We also describe various techniques to deal with the several parameters present in the proposed method, such as the location of the fictitious points, the source location in the MFS, and the estimation of a good value of the RBF shape parameter. Five numerical examples in 2D/3D and for second/fourth–order PDEs are presented and the performance of the proposed method is compared with that of the traditional MPS–MFS.

Keywords: method of fundamental solutions, method of particular solutions, radial basis functions, shape parameter, multiquadrics, fictitious points method

[*]School of Mathematical Sciences, University of Electronic Science and Technology of China

[†]Corresponding author. E-mail: fangfdou@uestc.edu.cn

[‡]Department of Mathematics and Statistics, University of Cyprus, P.O.Box 20537, 1678 Nicosia, Cyprus

[§]School of Mathematics and Natural Sciences, University of Southern Mississippi, USA

1 Introduction

During the past few decades, a great effort has been expended in the simplification of the various (tedious) mesh–based numerical methods such as finite element methods, finite difference methods, and finite volume methods. As a result, meshless methods have gained considerable popularity in scientific computing. The main attractive feature of meshless methods is that they alleviate the difficulties linked with expensive grid or element generation and the associated book–keeping of the mesh elements, particularly in the cases of complicated irregular domains, moving boundaries, or high–dimensional problems. The method of fundamental solutions (MFS) is a meshless method which has emerged as a popular and effective boundary–type technique which also belongs to the general class of boundary collocation methods. The MFS was first proposed by Kupradze and Aleksidze [18] in 1964 and, a few years later, Mathon and Johnston [20] introduced it as a numerical technique. Various applications to problems in science and engineering may be found in Fairweather and Karageorghis [6]. However, the MFS was confined to solving homogeneous partial differential equations (PDEs) until Golberg and Chen [13] in 1996 proposed the extension of the MFS to inhomogeneous PDEs in conjunction with radial basis functions (RBFs). We refer the reader to the survey papers [6, 7, 14] for further details regarding the development of the MFS.

A key feature in the extension of the MFS to inhomogeneous PDEs is the efficient evaluation of a particular solution of the given PDE. Over the years, various methods have been proposed for efficiently and accurately evaluating such a particular solution. The procedure of finding a particular solution is usually called *the method of particular solutions* (MPS). The combined scheme of first constructing a particular solution and then obtaining a solution to the corresponding homogeneous problem (an approach well-known in classical PDEs) with the MFS is called the MFS–RBF method [27] or the two-step MPS–MFS method [13]. This was the first approach employed where the MFS was used for solving linear inhomogeneous PDEs where the fundamental solution of the given differential operator is available. To further extend the combined MPS–MFS technique to a more general class of PDEs, a one–step MPS–MFS approach was proposed by directly combining the two sets of basis functions, i.e. the fundamental solutions of the homogeneous PDE (or part of the homogeneous PDE) and RBFs describing a particular solution [2,3,27]. As a result, the one–step MPS–MFS is capable of solving a much larger class of PDEs including ones involving variable coefficients [3].

In RBF collocation for fourth–order PDEs, in order to tackle the double boundary condition Fornberg [11] proposed a fictitious point method (FPM) in which an additional set of fictitious points is placed near the boundary (and outside the domain). In [10],

for second–order PDEs, in addition to fictitious points near the boundary, the governing equation is also collocated at boundary points. These fictitious points methods resemble the use of source points in the MFS, which are located outside the domain to avoid the singularity of the fundamental solutions. As shown in [19], the improvement in the accuracy obtained with the FPM is somehow limited. Consequently, the FPM has not been widely used in the RBFs community.

In this paper we propose improving the FPM by placing fictitious points in a fictitious domain containing the original domain. Recently, an improved version of the FPM has been developed in the context of the Kansa method [5]. As we shall see, the accuracy of this enhanced FPM improves considerably. Hence, for the first time, two distinct sets of fictitious points are employed simultaneously for the MFS and MPS. Moreover, the simplicity of the MFS for solving homogeneous PDEs is maintained and the resulting proposed method is truly meshless. It is noteworthy that the proposed approach may be applied to both the two–step and the one–step MPS–MFS. In this paper, we shall only focus on the one–step MPS–MFS.

The paper is organized in the following way. In Section 2, we briefly describe the particular solution approximation procedure using RBFs and the MFS for solving the homogeneous PDE, as well as the combined two–step MPS–MFS. In Section 3, the one–step MPS–MFS is presented while in Section 4, the fictitious points method is described. In Section 5, we discuss ways of selecting the various parameters involved in the proposed method in order to achieve optimal performance. In Section 6, five numerical examples in 2D/3D and for second/fourth–order PDEs are presented to show the robustness of the proposed technique. Finally, in Section 7, some conclusions and ideas for future work are provided.

2 Two-step MPS-MFS

In this section, we briefly review recent developments in the method of particular solutions step by step. We first consider the boundary value problem (BVP)

$$\mathcal{L}u(\mathbf{x}) = f(\mathbf{x}), \quad \mathbf{x} \in \Omega, \tag{1}$$

$$\mathcal{B}u(\mathbf{x}) = g(\mathbf{x}), \quad \mathbf{x} \in \partial\Omega, \tag{2}$$

where $\mathcal{L}$ is a linear elliptic partial differential operator, $\mathcal{B}$ is an operator specifying the boundary condition, $\Omega \subset \mathbb{R}^d$, $d = 2, 3$, is a bounded and connected domain with boundary $\partial\Omega$, and f, g are given functions.

One of the basic PDE approaches for solving BVP (1)–(2) is to first construct a particular solution u_p satisfying (1) without considering the boundary condition (2); i.e.,

$$\mathcal{L}u_p(\mathbf{x}) = f(\mathbf{x}). \tag{3}$$

The homogeneous solution is then obtained by solving the homogeneous PDE

$$\mathcal{L}u_h(\mathbf{x}) \;=\; 0, \quad \mathbf{x} \in \Omega, \tag{4}$$

subject to

$$\mathcal{B}u_h(\mathbf{x}) \;=\; g(\mathbf{x}) - \mathcal{B}u_p(\mathbf{x}), \quad \mathbf{x} \in \partial\Omega. \tag{5}$$

Once u_p and u_h are known, the solution of BVP (1)–(2) can be obtained from $u = u_h + u_p$.

Various numerical methods, both mesh–based and meshless, have been developed to calculate the particular and homogeneous solutions. Atkinson [1] proposed three different approaches for the construction of an approximate particular solution in the case $\mathcal{L} \equiv \Delta$. However, deriving a closed–form particular solution for general differential operators remains a challenge. Among all numerical methods, RBF techniques have become very popular for the evaluation of particular solutions. Once an approximate particular solution has been constructed, various boundary methods may be employed for the approximation of the homogeneous solution corresponding to BVP (4)–(5). In the current paper, we will choose the multiquadric (MQ) RBFs ($\sqrt{1+r^2c^2}$, where c is the shape parameter), which are considered as one of the most effective RBFs, as the basis functions for the evaluation of the approximate particular solution, and the MFS [6, 14] for the approximation of the homogeneous solution.

2.1 Approximation of particular solution

In this subsection, we describe the RBF collocation method for the evaluation of an approximate particular solution of (3). An analytical particular solution in (3) can be obtained only for very simple cases of $f(\mathbf{x})$ and $\mathcal{L}$. In general, a numerical approach is required for such a purpose. Let $\{\mathbf{x}_j\}_{j=1}^n$ be a set of points inside (or even outside) the domain Ω. We first approximate f in (3) as follows:

$$f(\mathbf{x}) \simeq \hat{f}(\mathbf{x}) = \sum_{j=1}^{n} a_j \phi_j(\mathbf{r}), \tag{6}$$

where $\phi_j(\mathbf{r}) = \phi(\|\mathbf{x} - \mathbf{x}_j\|)$ is an RBF. The unknown coefficients $\{a_j\}$ can be determined by solving the square linear system resulting from the collocation equations

$$\sum_{j=1}^{n} a_j \phi_j(\mathbf{r}_k) = f(\mathbf{x}_k), \quad k = 1, 2, \cdots, n, \tag{7}$$

where now $\phi_j(\mathbf{r}_k) = \phi(\|\mathbf{x}_k - \mathbf{x}_j\|)$. An approximate particular solution $\hat{u}_p$ of (3) can then be obtained from

$$\hat{u}_p(\mathbf{x}) = \sum_{j=1}^{n} a_j \Phi_j(\mathbf{r}), \tag{8}$$

where

$$\mathcal{L}\Phi = \phi. \tag{9}$$

A major challenge in the evaluation of a particular solution is the derivation of a closed–form particular solution Φ in (9). Throughout the paper we shall denote the shape parameter by c, and as is well–known it needs to be carefully selected in order to achieve optimal performance. We will explain how to calculate an appropriate value of the shape parameter later. With $\phi(r) = \sqrt{1 + r^2c^2}$ (MQ) and $\mathcal{L} \equiv \Delta$ (Laplacian), the closed–form particular solutions $\Phi(r)$ in (9) are available as follows [21]:

$$\Phi(r) = \begin{cases} \dfrac{1}{9c^2}\left((4 + c^2r^2)\phi(r) - 3\ln\left(1 + \phi(r)\right)\right), & \text{in 2D,} \\ \begin{cases} \dfrac{5 + 2c^2r^2}{24c^2}\phi(r) + \dfrac{\sinh^{-1}(cr)}{8c^3 r}, & r > 0, \\ \dfrac{1}{3c^2}, & r = 0. \end{cases} & \text{in 3D,} \end{cases} \tag{10}$$

For $\mathcal{L} \equiv \Delta^2$ (biharmonic), in 2D we have [21]

$$\Phi(r) = \frac{2 - 5c^2r^2}{60c^4}\ln\left(1 + \phi(r)\right) + \frac{\phi(r)}{900c^4}\left(4c^4r^4 + 48c^2r^2 - 61\right) + \frac{2c^2r^2 + 1}{24c^4}, \tag{11}$$

while in 3D, we have [21]

$$\Phi(r) = \begin{cases} \dfrac{\phi(r)}{1440c^4}\left(4c^4r^4 + 28c^2r^2 - 81\right) + \dfrac{\sinh^{-1}(cr)}{96c^5 r}\left(6c^2r^2 - 1\right), & r > 0, \\ \dfrac{-1}{15c^4}, & r = 0. \end{cases} \tag{12}$$

For $\mathcal{L}$ different than Δ or Δ^2, we can still use Φ from (10)–(12) for the evaluation of the particular solutions. For instance, when $\mathcal{L} \equiv \Delta + \alpha\partial/\partial x + \beta\partial/\partial y + \gamma$, where α, β, and γ are constants, substituting (8) into (3), we obtain

$$\begin{aligned} \mathcal{L}\hat{u}_p(\mathbf{x}) &= \sum_{j=1}^{n} a_j \left(\phi_j(\mathbf{r}) + \alpha\frac{\partial\Phi_j(\mathbf{r})}{\partial x} + \beta\frac{\partial\Phi_j(\mathbf{r})}{\partial y} + \gamma\Phi_j(\mathbf{r})\right) \\ &= f(\mathbf{x}). \end{aligned} \tag{13}$$

The unknown coefficients $\{a_j\}$ in (13) can be easily obtained by the collocation method described earlier and the approximate particular solution $\hat{u}_p$ can be evaluated from (8). For other differential operators $\mathcal{L}$, a particular solution $\hat{u}_p$ can be obtained in a similar way.

2.2 The method of fundamental solutions

Once an approximate particular solution u_p in (3) is available, we can proceed to solve the homogeneous problem (4)–(5) using the MFS which, for completeness, we briefly describe.

Let $\{\mathbf{x}\}_{k=1}^m$ be a set of collocation points on the boundary $\partial\Omega$ and $\{\boldsymbol{\xi}_k\}_{k=1}^m$ a set of source points located outside $\overline{\Omega}$. The reason for moving the source points outside the domain is to avoid the singularity of the fundamental solution of $\mathcal{L}$. For second–order elliptic PDEs, the solution of (4)–(5) is approximated by a linear combination of fundamental solutions in the form [6, 14]

$$u_h(\mathbf{x}) \simeq \hat{u}_h(\mathbf{x}) = \sum_{k=1}^{m} c_k\, G_k(\boldsymbol{\rho}), \quad \mathbf{x} \in \overline{\Omega}, \tag{14}$$

where $G_k(\rho) = G(\|\mathbf{x} - \boldsymbol{\xi}_k\|)$ and G is the fundamental solution of the operator $\mathcal{L}$ in (4). There are various ways of selecting the source points [4] and this will be briefly discussed in the next section.

The unknown coefficients $\{c_k\}$ in (14) can be determined by a collocation method. Using (14) in collocating boundary condition (5), we obtain a square linear system from the equations

$$\sum_{k=1}^{m} c_k\, \mathcal{B}G_k(\boldsymbol{\rho}_j) = g(\mathbf{x}_j) - \mathcal{B}u_p(\mathbf{x}_j), \quad j = 1, 2, \cdots, m. \tag{15}$$

After the coefficients $\{c_k\}$ have been obtained, the approximate homogeneous solution $\hat{u}_h$ can be evaluated from (14). Note that although the system matrix resulting from (15) is poorly–conditioned, for smooth boundaries and boundary conditions, the accuracy of the numerical solution remains largely unaffected.

Once the approximate particular solution $\hat{u}_p$ and the approximate homogeneous solution $\hat{u}_h$ are available, the approximate solution of the original BVP (1)–(2) can be computed at any given point in Ω.

For fourth–order PDEs such as $\mathcal{L}u(\mathbf{x}) \equiv \Delta^2 u(\mathbf{x}) = 0$ in which two boundary conditions are required, approximation (14) is replaced by [16]

$$u_h(\mathbf{x}) \simeq \hat{u}_h(\mathbf{x}) = \sum_{k=1}^{m} c_k G_k(\boldsymbol{\rho}) + \sum_{k=1}^{m} d_k \mathcal{G}_k(\boldsymbol{\rho}), \quad \mathbf{x} \in \overline{\Omega}, \tag{16}$$

where $G(\boldsymbol{\rho})$ and $\mathcal{G}(\boldsymbol{\rho})$ are the fundamental solutions of Δ and Δ^2, respectively. Since there are two boundary conditions at each boundary point, the matrix resulting from the collocation of the boundary conditions is square.

The above solution procedure is well–documented in the literature. The MFS was employed for the solution of inhomogeneous equations through the use of RBFs and two–step classical solution procedure described above. This is considered a major leap in the development of the MFS. A remaining major hurdle, however, is that the two–step procedure is restricted to a limited class of partial differential equations for which the fundamental solutions are available. In recent years, the two–step solution procedure has evolved to a one–step procedure which enabled researchers to solve a larger class of PDEs [3, 8, 15, 21]. In the next section, we shall briefly describe an one–step solution procedure using the MPS and MFS.

3 One-step MPS-MFS

Without loss of generality, let us consider BVP (1)–(2) in 2D with

$$\mathcal{L} \equiv \Delta + \widetilde{\mathcal{L}}, \tag{17}$$

where $\widetilde{\mathcal{L}}$ is a linear operator of order at most two. For example, we could have

$$\widetilde{\mathcal{L}} \equiv \alpha(\mathbf{x})\frac{\partial}{\partial x} + \beta(\mathbf{x})\frac{\partial}{\partial y} + \gamma(\mathbf{x}),$$

where $\alpha(\mathbf{x}), \beta(\mathbf{x})$, and $\gamma(\mathbf{x})$ are known functions.

In 3D, a similar procedure can be applied.

For the one–step approach as described in [3, 8, 15, 21], the solution is approximated by the sum of the particular solution $\hat{u}_p$ in (8) and the homogeneous solution $\hat{u}_h$ in (14) as follows:

$$u(\mathbf{x}) \simeq \hat{u}(\mathbf{x}) = \sum_{j=1}^{n} a_j \Phi_j(\mathbf{r}) + \sum_{k=1}^{m} c_k G_k(\boldsymbol{\rho}). \tag{18}$$

As shown in [8, 21], the Laplacian Δ in (17) is treated as the major differential operator and the remaining terms are moved to the right hand side. This means that the given differential equation can be rearranged as the following Poisson-type equation:

$$\Delta u = -\widetilde{\mathcal{L}}u + f(x, y), \quad (x, y) \in \Omega. \tag{19}$$

As such, the closed–form particular solution Φ in (10) can be used in (19) while the fundamental solution is $\ln \boldsymbol{\rho}$ in 2D (and $1/\boldsymbol{\rho}$ in 3D). Since $\Delta G(\boldsymbol{\rho}) = 0$, and $\Delta\Phi = \phi$, for $(x, y) \in \Omega$, from (18) we have

$$\Delta u \simeq \Delta \hat{u} = \sum_{j=1}^{n} a_j \phi_j(\mathbf{r}).$$

Substituting (18) into (19), we get

$$\sum_{j=1}^{n} a_j \Psi_j(\mathbf{r}) + \sum_{k=1}^{m} c_k \Xi_k(\boldsymbol{\rho}) = f(x, y), \quad \text{for (x, y)} \in \Omega, \tag{20}$$

where

$$\Psi_j(\mathbf{r}) = \phi_j(\mathbf{r}) + \widetilde{\mathcal{L}}\Phi_j(\mathbf{r}),$$

and

$$\Xi_k(\boldsymbol{\rho}) = \widetilde{\mathcal{L}}G_k(\boldsymbol{\rho}).$$

Furthermore, from boundary condition (2), we obtain

$$\sum_{j=1}^{n} a_j \mathcal{B}\Phi_j(\mathbf{r}) + \sum_{k=1}^{m} c_k \mathcal{B}G_k(\boldsymbol{\rho}) = g(x, y), \quad (x, y) \in \partial\Omega. \tag{21}$$

Using n centres, m boundary points, and m source points outside $\overline{\Omega}$, we can determine the unknown coefficients $\{a_j\}$ and $\{c_k\}$ by the standard collocation method. More specifically, we collocate (20) at n interior points and (21) at the m boundary points yielding $m + n$ equations in $m + n$ unknowns. Note that the n interior points where (20) is collocated are not necessarily the same as the centres. Moreover, we could collocate (20) at a *combination* of n interior and boundary points. Once the coefficients have been determined, the approximate solution at any given point in $\overline{\Omega}$ can be evaluated using (18).

Let us now consider the fourth–order BVP

$$\mathcal{L}u(\mathbf{x}) = f(\mathbf{x}), \quad \mathbf{x} \in \Omega, \tag{22}$$

$$\mathcal{B}_1 u(\mathbf{x}) = g_1(\mathbf{x}), \quad \mathbf{x} \in \partial\Omega, \tag{23}$$

$$\mathcal{B}_2 u(\mathbf{x}) = g_2(\mathbf{x}), \quad \mathbf{x} \in \partial\Omega, \tag{24}$$

with $\mathcal{L} \equiv \Delta^2 + \widetilde{\mathcal{L}}$, where $\widetilde{\mathcal{L}}$ is a linear operator of order at most four. Also, $\mathcal{B}_1$ and $\mathcal{B}_2$ are operators specifying the boundary conditions. Instead of approximation (18) we now have

$$u(\mathbf{x}) \simeq \hat{u}(\mathbf{x}) = \sum_{j=1}^{n} a_j \Phi_j(\mathbf{r}) + \sum_{k=1}^{m} c_k G_k(\boldsymbol{\rho}) + \sum_{k=1}^{m} d_k \mathcal{G}_k(\boldsymbol{\rho}), \tag{25}$$

where Φ is given by (11) in the 2D case and (12) in the 3D case, and $G_k(\boldsymbol{\rho})$ and $\mathcal{G}_k(\boldsymbol{\rho})$ are the fundamental solutions of Δ and Δ^2, respectively. From (22) and (25) we get

$$\sum_{j=1}^{n} a_j \Psi_j(\mathbf{r}) + \sum_{k=1}^{m} c_k \Xi_k(\boldsymbol{\rho}) + \sum_{k=1}^{m} d_k \Upsilon_k(\boldsymbol{\rho}) = f(x, y), \quad \text{for } (\mathrm{x}, \mathrm{y}) \in \Omega, \tag{26}$$

where

$$\Psi_j(\mathbf{r}) = \phi_j(\mathbf{r}) + \widetilde{\mathcal{L}} \Phi_j(\mathbf{r}),$$

and

$$\Xi_k(\boldsymbol{\rho}) = \widetilde{\mathcal{L}} G_k(\boldsymbol{\rho}), \quad \Upsilon_k(\boldsymbol{\rho}) = \widetilde{\mathcal{L}} \mathcal{G}_k(\boldsymbol{\rho}).$$

Moreover, from boundary conditions (23) and (24) we obtain

$$\sum_{j=1}^{n} a_j \mathcal{B}_1 \Phi_j(\mathbf{r}) + \sum_{k=1}^{m} c_k \mathcal{B}_1 G_k(\boldsymbol{\rho}) + \sum_{k=1}^{m} d_k \mathcal{B}_1 \mathcal{G}_k(\boldsymbol{\rho}) = g_1(x, y), \quad (x, y) \in \partial\Omega, \tag{27}$$

and

$$\sum_{j=1}^{n} a_j \mathcal{B}_2 \Phi_j(\mathbf{r}) + \sum_{k=1}^{m} c_k \mathcal{B}_2 G_k(\boldsymbol{\rho}) + \sum_{k=1}^{m} d_k \mathcal{B}_2 \mathcal{G}_k(\boldsymbol{\rho}) = g_2(x, y), \quad (x, y) \in \partial\Omega, \tag{28}$$

respectively. As in the second–order case, we choose n centres, m boundary points, and m source points outside $\overline{\Omega}$. The unknown coefficients $\{a_j\}$, $\{c_k\}$ and $\{d_k\}$ can be determined by collocating (26) at n interior points (or a combination of n interior and boundary points) and (27) and (28) at the m boundary points yielding $2m+n$ equations in $2m + n$ unknowns.

The above one–step MPS–MFS formulation can be used to solve a much larger class of PDEs including ones with variable coefficients. As already stated, in this study, we will focus on the one–step approach.

4 Fictitious points method

In this section, we propose a technique which uses *fictitious or ghost* points and which further enhances the performance of the one–step MPS–MFS approach. Such techniques

are often employed to enforce the two boundary conditions in fourth–order PDEs in finite difference methods. Fornberg [11] applied such an approach for global collocation methods. For second–order PDEs, an improved Kansa–MQ method with collocation of the PDE on the boundary (MQ PDECV) was used in [10, 19, 23]. More specifically, fictitious nodes adjacent to the boundary were added and both the boundary condition and the PDE were collocated at the boundary points. Results in [10] showed some improvement when using the MQ PDECV while results in [19] showed otherwise.

In this section, we are moving one step further by proposing an improved fictitious points method. In our approach, we distribute the fictitious (or ghost) points as uniformly as possible inside and outside the domain. The shape of the region covering these fictitious points can be arbitrary. For convenience, we choose these fictitious points to lie inside a circle/sphere covering the domain in 2D/3D. Figure 1 shows the distribution of fictitious (red •), boundary (blue •), and interior (green •) points of the MQ PDECV [19, 23] and our proposed approach. Note that the distributions of the fictitious points in these two approaches are fundamentally different. In MQ PDECV, the number of fictitious points in Figure 1(a) is equal to the number of boundary points, while in the proposed approach, the number of fictitious points is equal to sum of interior and boundary points as shown in Figure 1(b). Furthermore, in our approach, the fictitious points are distributed as uniformly as possible inside a circle (in 2D). For instance, these points are distributed in a *sunflower* structure. We refer readers to [26] for the detailed construction of *sunflower points*. The MATLAB© code for generating these uniformly distributed sunflower points can be easily obtained from the internet. For the 3D case, we use quasi–random points inside a sphere to ensure the fictitious points are fairly uniformly distributed (the code `haltonset` is available in MATLAB©). We will further elaborate on how to choose the radius of the uniformly distributed points in a circle/sphere in the numerical results section.

Our proposed fictitious points method is quite different than the above mentioned methods. For second–order PDEs, we can either include or exclude the boundary points from the centres in the RBF particular solution approximation. For fourth–order PDEs, the linear combination of fundamental solutions G and $\mathcal{G}$ (of the Laplacian and bi-harmonic operators, respectively) as shown in (25) allows us to handle two boundary conditions ensuring that the resulting matrix is square.

Moreover, the centres (ghost points) and collocation points are two completely different sets of points and the centers can be distributed in an arbitrary way inside and outside the domain. As we shall see in the numerical results section, various ways of selecting the fictitious points are possible. This type of node distribution bears a striking resemblance to the use of source points in the MFS except for the fact that the latter

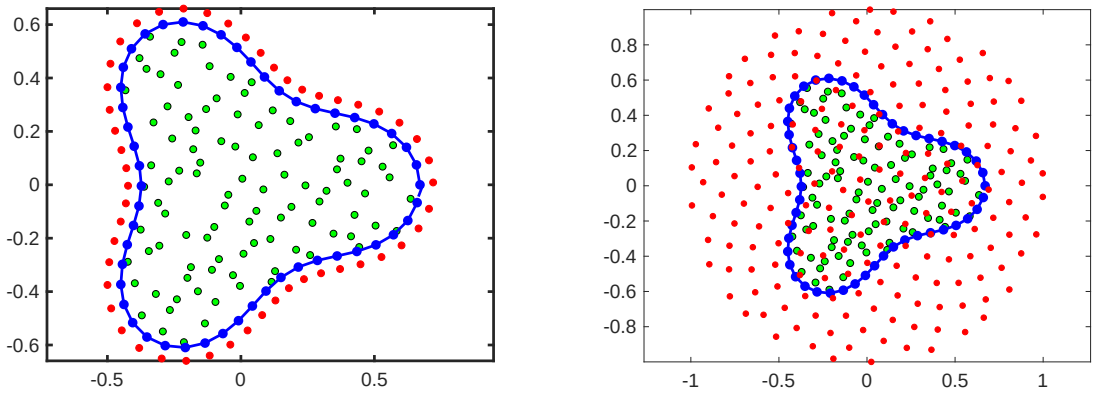

(a) (b)

Figure 1: The profiles of the distribution of fictitious (red •), boundary (blue •), and interior (green •) points (a) for the MQ PDECV method, and (b) for the proposed method.

cannot be placed inside the closure of the domain. Hence, this is the first time that the two methods (MPS and MFS) are combined into one and both have their respective fictitious points in the solution process.

5 Determination of parameters

There are several parameters requiring special attention in the fictitious points one–step MPS–MFS method. The selection algorithms for some of these parameters are well–developed and can be found in the literature. Firstly, the determination of the RBF shape parameter is a challenging issue which is problem dependent. Despite many efforts, the optimal selection of the shape parameter remains an outstanding research topic. Among all the available techniques, the LOOCV (Leave-One-Out Cross Validation) algorithm [22] is widely considered to be an effective method for the selection of the RBF shape parameter. Since the method has become rather standard, we will not further elaborate on it and simply refer the reader to [22] for further details. In the implementation of LOOCV, one of the issues is the selection of an initial search interval `[min, max]` [9]. It is also known that the modified Franke formula $c = 0.8\sqrt[4]{\mathcal{N}}/D$, where D is the diameter of the smallest circle containing all $\mathcal{N}$ collocation points [12,17], provides a good estimate of the shape parameter. We further modified Franke's formula by replacing D by the radius of the ghost circle/sphere and used it as an initial predictor. Then we chose `min` $= \max(0, c-\varepsilon]$, `max` $= c+\varepsilon$. After intensive experimentation, we deduced that ε can take

any value between 0.4 and 0.8 and, as a result, in this paper, we take $\varepsilon = 0.5$. Combining these two approaches, we can form a more reliable hybrid method for the selection of the shape parameter in a predictor–corrector sense.

Secondly, the determination of the location of the source points in the MFS is also critical for optimal numerical performance. As is the case with the shape parameter in the RBFs, the optimal selection of the source points is also an active research topic. Currently, there are many algorithms proposed for this purpose [4]. Among all the proposed selection algorithms, two are very simple: (1) Placing the source points on a circle/sphere in 2D/3D and (2) placing the source points on a curve/surface (2D/3D) similar to the shape of the boundary as illustrated in Figure 2 . For simplicity, we will adopt the circle/sphere approach in which its radius can be determined by the LOOCV algorithm. We refer the reader to [4, 24, 25] for further details.

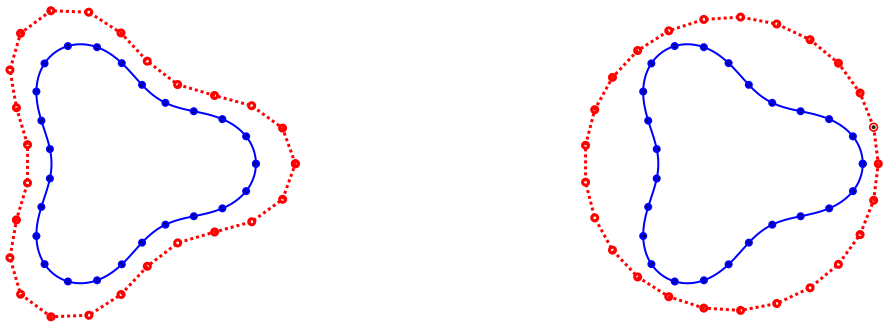

(a) (b)

Figure 2: Two typical distributions of the MFS source points (red •) in 2D.

Thirdly, in the fictitious points method proposed in Section 4 , Halton quasi–random points covering the domain are employed to ensure the fairly uniform distribution of the fictitious points (see Figure 1(b)). The number of fictitious points used for RBFs is equal to the sum of the number of interior and boundary points. The determination of the radius of the fictitious circle/sphere covering the domain will be further investigated later. We will conduct a series of numerical tests in the next section for a better understanding of this issue. In Figure 3, we added the source points of the MFS in black (•) to Figure 1(b). In most of our numerical examples, we will use LOOCV to determine the radius of the source circle [4]. In the next section, we will discuss how to distribute the fictitious points to achieve optimal performance in more detail.

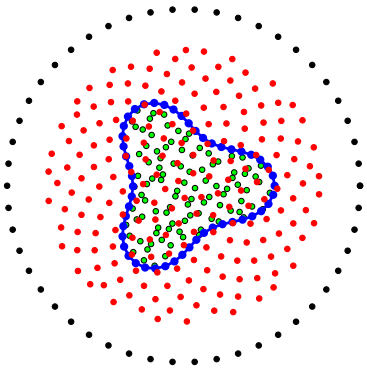

Figure 3: The profiles of the distribution of the RBF fictitious (red •), boundary points (blue •), interior points (green •), and source points of the MFS (black •) for the proposed method.

6 Numerical results

To demonstrate the effectiveness of the current method, five examples are presented in this section. In each example, we compare the numerical results obtained with the proposed method with those obtained using the traditional one–step MPS–MFS technique [2, 3, 27].

Through this section, we denote by N_i, N_b, N_s, N_t, and N_g the number of interior points, boundary points, source points, test points, and ghost points, respectively. We will add the boundary points to the interior points in the RBF interpolation of the particular solution formulation as shown in the first term on the right hand side of (18); i.e., $n = N_i + N_b$ and $m = N_b$. Thus, in the second–order case we shall have square systems of order $(N_i + 2N_b)$ while in the fourth–order case we shall have square systems of order (N_i+3N_b). All these points are distributed uniformly using Halton quasi-random points (from the MATLAB© command `haltonset`).

To measure the accuracy of the approximate solution we calculated the root–mean–squared error (RMSE)

$$RMSE = \sqrt{\frac{1}{N_t}\sum_{j=1}^{N_t}(\hat{u}_j - u_j)^2}$$

where $\hat{u}_j$ and u_j are the approximate and exact solutions respectively.

Example 1 We first consider the second–order BVP

$$(\Delta + \frac{\partial}{\partial y} - x^2 y)u(x,y) = f(x,y), \quad (x,y) \in \Omega, \tag{29}$$

$$u(x,y) = g_1(x,y), \quad (x,y) \in \partial\Omega_1, \tag{30}$$

$$\frac{\partial}{\partial n}u(x,y) = g_2(x,y), \quad (x,y) \in \partial\Omega_2, \tag{31}$$

where $f(x,y)$, $g_1(x,y)$ and $g_2(x,y)$ are obtained from the exact solution

$$u(x,y) = \mathrm{e}^{2x}\cos(y^2 + x). \tag{32}$$

The computational domain Ω is defined by the parametric equation

$$\Omega = \{(x,y)|x = \rho(t)\cos(t), y = \rho(t)\sin(t), 0 \le t \le 2\pi\},$$

where

$$\rho(t) = \mathrm{e}^{\sin(t)}\sin^2(2t) + \mathrm{e}^{\cos(t)}\cos^2(2t).$$

The boundary segments $\partial\Omega_1$ and $\partial\Omega_2$ denote the Dirichlet and Neumann boundary respectively, and $\partial\Omega = \partial\Omega_1 \bigcup \partial\Omega_2$, $\partial\Omega_1 \bigcap \partial\Omega_2 = \varnothing$. The domain and its boundary are shown in Figure 4(a), and the profile of the exact solution is shown in Figure 4(b).

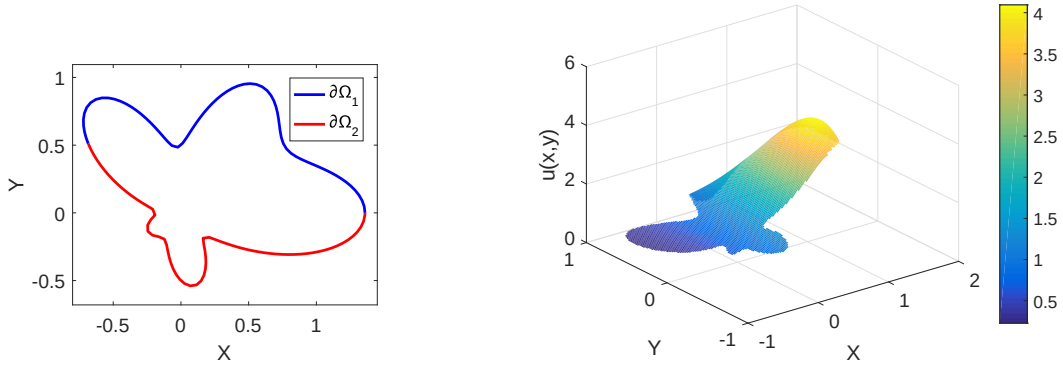

(a) (b)

Figure 4: Example 1. The profiles of (a) the amoeba domain and (b) the exact solution.

In the numerical implementation, we chose $N_i = 400$, 100 boundary points where the Dirichlet boundary condition is imposed, and 100 boundary points where the Neumann boundary condition is imposed. Hence, we have $N_b = 200$, $N_s = N_b$, $N_g = N_i + N_b = 600$

and the length of the Dirichlet boundary is equal to the length of Neumann boundary. We took the radius R of the ghost circle to be 2.

The numerical results obtained using the proposed method are compared with those obtained using the traditional MPS–MFS method. All conditions are the same except for the fact that the centres of the proposed method are now ghost points. The RMSE was evaluated at 200 scattered test points. The numerical results using different shape parameter (c) values are presented in Figure 5(a) from which it is evident that the proposed method is far superior to the traditional method. Note that in Figure 5(a) the radii $\mathcal{R}$ of the MFS source circles are obtained using LOOCV (see [4]) for each value of the shape parameter c. As a result we are not able to show these in the figure.

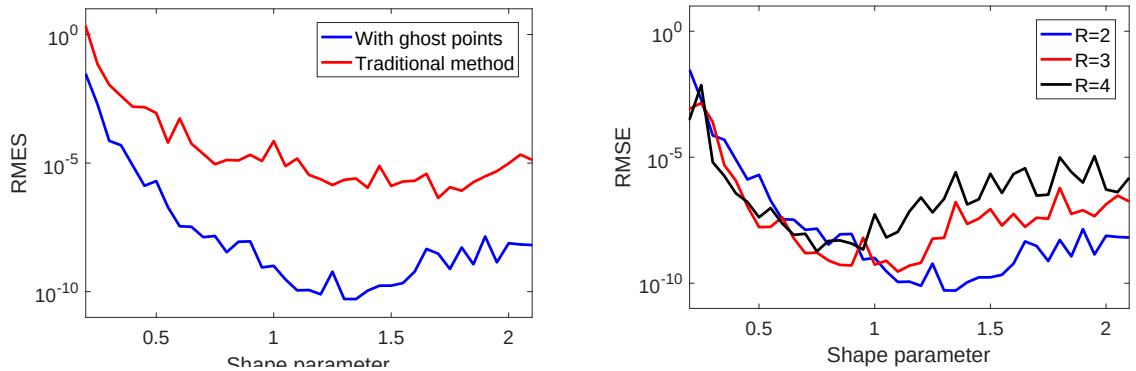

(a) (b)

Figure 5: Example 1. The profiles of the (a) RMSE by using present the method and the traditional method for the case $R = 2$. (b) RMSE by using different radii of the ghost circle.

Furthermore, we studied the impact of the size of the ghost circle on accuracy and the results are shown in Figure 5(b). It is clear that the proposed method's accuracy and the optimal shape parameter of the normalized MQ are reduced when the radius R of the ghost circle becomes larger. Let $\mathcal{R}$ be the radius of the source circle which can be obtained by LOOCV as shown in [4]. The results obtained with different radii R and $\mathcal{R}$ using LOOCV and the modified Franke formula are presented in Table 1. From the cases $R = 2$, 3 and 4, we observe that the results in Table 1 are consistent with those in Figure 5(b). Moreover, from Table 1, it is evident that the length of the radius of the ghost circle has a significant effect on the accuracy of the method.

Table 1: Example 1: Shape parameter and RMSE for different radii R and $\mathcal{R}$ using LOOCV and the modified Franke formula.

LOOCV				Franke		
R	$\mathcal{R}$	c	RMSE	c	$\mathcal{R}$	RMSE
1.5	5.326	1.169	1.060(-08)	1.320	6.347	2.247(-09)
2	3.747	1.447	1.113(-10)	0.990	6.250	2.562(-09)
2.5	5.087	0.793	2.929(-09)	0.792	6.307	6.260(-10)
3	3.136	1.014	1.542(-09)	0.660	3.375	3.221(-09)
3.5	6.758	0.622	9.435(-09)	0.566	5.382	9.579(-09)
4	3.674	0.696	1.757(-09)	0.495	4.551	1.236(-07)
4.5	4.998	0.650	1.384(-08)	0.440	3.346	4.957(-07)

Example 2 We next consider the fourth–order BVP

$$(\Delta^2 - 9\Delta + x^2 y)u(x,y) = f(x,y), \quad (x,y) \in \Omega, \tag{33}$$

$$\Delta u(x,y) = g_1(x,y), \quad (x,y) \in \partial\Omega, \tag{34}$$

$$u(x,y) = g_2(x,y), \quad (x,y) \in \partial\Omega, \tag{35}$$

where $f(x,y)$, $g_1(x,y)$ and $g_2(x,y)$ are given functions calculated from the exact solution

$$u(x,y) = \sin(\pi x)\cosh y - \cos(\pi x)\sinh y.$$

The gear–shaped domain Ω is defined by the parametric equation

$$\Omega = \{(x,y) | x = \rho(t)\cos(\theta(t)), y = \rho(t)\sin(\theta(t)), 0 \le t \le 2\pi\},$$

where

$$\rho(t) = 2 + \frac{1}{2}\sin(6t), \quad \theta(t) = t + \frac{1}{2}\sin(6t).$$

The domain and its boundary are shown in Figure 6(a) while the profile of the exact solution is presented in Figure 6(b).

In the numerical implementation, we took $N_i = 400$, $N_b = 200$, $N_t = 200$, and the radius of the ghost circle was set to 2.5. As in Example 1, the radius of the MFS source circle was obtained using LOOCV for each value of the shape parameter. The numerical results corresponding to different values of the shape parameter in the proposed and traditional methods are shown in Figure 7 where, again, the superiority of the proposed method is evident.

In Table 2, we list the results obtained with different radii of the ghost circle R when using LOOCV and the modified Franke formula. From these numerical results, we can

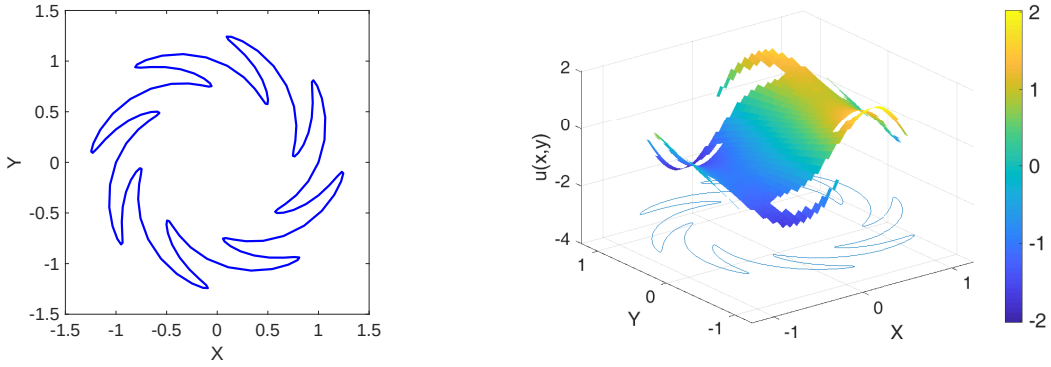

(a) (b)

Figure 6: Example 2. The profiles of (a) the gear domain, (b) the exact solution.

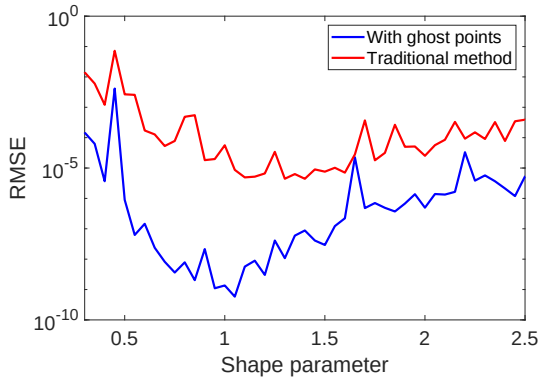

Figure 7: Example 2. The profiles of RMSE for different shape parameter values in the proposed and traditional methods.

see that the radius R has a significant influence on the accuracy of the method. In this example when R is less than 2.5, the accuracy of numerical results decreases as R becomes smaller, and when R is greater than 2.5, the accuracy of numerical results also begins to deteriorate as R becomes larger.

Example 3 We next consider the 3D second–order BVP

$$(\Delta + y\frac{\partial}{\partial x} + x\cos y - 100)u(x,y,z) = f(x,y,z), \quad (x,y,z) \in \Omega, \tag{36}$$

$$u(x,y,z) = g(x,y,z), \quad (x,y,z) \in \partial\Omega, \tag{37}$$

where f and g are given functions obtained from the exact solution

$$u(x,y,z) = \mathrm{e}^{2x}\sin y + \mathrm{e}^{2x}\cos z.$$

Table 2: Example 2: Shape parameter and RMSE for different radii of R and $\mathcal{R}$ using LOOCV and the modified Franke formula.

	LOOCV			Franke		
R	c	$\mathcal{R}$	RMSE	c	$\mathcal{R}$	RMSE
1.5	0.966	6.348	7.079(-06)	1.320	4.315	2.578(-08)
2	0.913	5.310	6.475(-08)	0.990	5.259	7.898(-09)
2.5	0.987	3.130	8.640(-10)	0.792	4.222	6.187(-09)
3	0.730	4.633	3.849(-09)	0.660	5.116	1.018(-08)
3.5	0.658	5.164	5.514(-09)	0.566	3.202	5.900(-08)
4	0.687	4.724	9.428(-09)	0.495	6.341	3.405(-07)
4.5	0.629	5.113	2.368(-08)	0.440	5.326	1.789(-07)

As shown in Figure 8, Ω is a gear–shaped domain in 3D. In the numerical implementation,

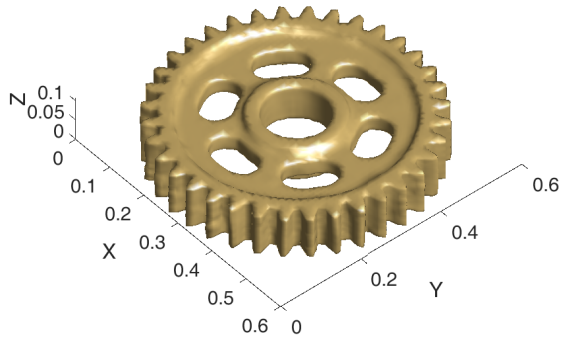

Figure 8: Example 3. The profile of the 3D gear–shaped domain.

we took $N_i = 1000$, $N_b = 419$, $N_t = 354$, and the radius of the ghost sphere R to be 1.5. The cloud boundary data points for $\partial\Omega$ are available from the website [30].

Due to the large number of collocation points, using LOOCV to find the optimal MFS source circle radius $\mathcal{R}$ becomes very time–consuming. In Table 3 we show the accuracy of the method using various radii $\mathcal{R}$. Unlike the MQ shape parameter, we found that the radius of the source sphere has little effect on the accuracy. Therefore, in this and the next 3D examples, we will preset a value of $\mathcal{R}$. In this example, we set $\mathcal{R} = 5$. The numerical results corresponding to different shape parameters c in the proposed and traditional methods are shown in Figure 9.

The results are similar to those in the 2D examples and the accuracy of the proposed

Table 3: Example 3: RMSE for various $\mathcal{R}$ with fixed shape parameter $c = 3.306$.

$\mathcal{R}$	RMSE	$\mathcal{R}$	RMSE
2	5.704(-09)	5	2.162(-10)
3	7.339(-10)	6	2.887(-10)
4	3.499(-10)	7	1.724(-09)

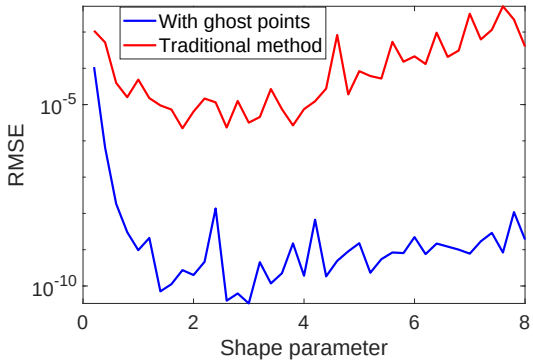

Figure 9: Example 3. The profiles of RMSE for different shape parameters of the proposed and traditional methods using $\mathcal{R} = 5$.

method is far superior to that of the traditional one–step MPS–MFS.

The results for different radii of the ghost sphere R using LOOCV and the modified Franke formula are shown in Table 4. In the 2D examples, the computational costs of LOOCV and the modified Franke formula are similar. However, in the 3D cases, the computational cost of LOOCV is substantially higher as shown in Table 4. From these numerical results it is clear that LOOCV has the advantage of better accuracy over Franke's formula but this comes at a high computational cost.

Example 4 Here we consider the fourth–order 3D BVP

$$(\Delta^2 - 1000\Delta + xyz)u(x,y,z) = f(x,y,z), \quad (x,y,z) \in \Omega, \tag{38}$$

$$\frac{\partial^2}{\partial n^2}u(x,y,z) = g_1(x,y,z), \quad (x,y,z) \in \partial\Omega, \tag{39}$$

$$u(x,y,z) = g_2(x,y,z), \quad (x,y,z) \in \partial\Omega, \tag{40}$$

where f, g_1, and g_2 are calculated from the exact solution

$$u(x,y,z) = \mathrm{e}^{2x}\sin y \cos z.$$

Table 4: Example 3: Shape parameter and RMSE for different radii of the ghost spheres using LOOCV and the modified Franke formula.

	LOOCV			Franke		
R	c	RMSE	CPU(s)	c	RMSE	CPU(s)
1	3.306	2.162(-10)	7.71	2.455	1.544(-09)	0.59
1.5	2.668	7.334(-11)	4.63	1.637	3.704(-10)	0.64
2	1.798	3.074(-11)	7.88	1.227	4.177(-10)	0.61
2.5	1.263	5.521(-10)	7.78	0.982	3.730(-09)	0.63
3	1.039	1.385(-09)	8.41	0.818	9.102(-10)	0.67
3.5	1.175	1.100(-10)	8.34	0.701	3.068(-09)	0.71
4	1.183	2.867(-10)	7.13	0.618	7.459(-10)	0.72
4.5	1.134	5.642(-09)	7.73	0.546	1.079(-08)	0.61

and Ω is the Stanford Bunny whose boundary cloud points and their normals are available from the Stanford three–dimensional scanning repository [29]. Since the scale of the original data is too small, in our numerical implementation we multiply these data by 10. The profile of the Stanford Bunny and its boundary points are shown in Figure 10.

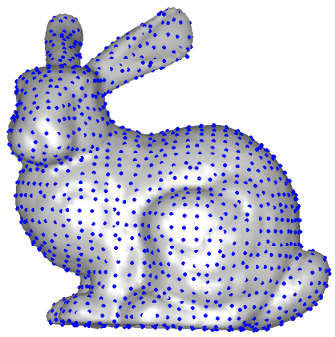

Figure 10: Example 4. The profiles of Stanford bunny.

We set $N_i = 1000$, $N_b = 470$, $N_t = 334$, $\mathcal{R} = 5$, and the ghost sphere radius R to be 3. In Figure 11, we present the numerical results corresponding to different shape parameters for the current and traditional one–step MPS–MFS methods.

In Table 5, we list the results obtained for different radii R of the ghost sphere obtained by using LOOCV and the modified Franke formula. As we can see, the results obtained with LOOCV are slightly better than those obtained with the modified Franke

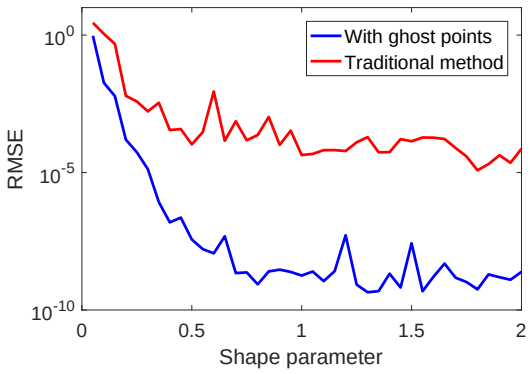

Figure 11: Example 4. The profiles of RMSE for different shape parameters for the current and traditional methods.

formula at the expense of a much higher computational cost. The results using these two approaches for finding a good shape parameter are consistent and offer an independent confirmation for the final results, particularly when no exact solution is available.

Table 5: Example 4: Shape parameter and RMSE for different radii of the ghost sphere using LOOCV and the modified Franke formula.

	LOOCV		Franke	
R	c	RMSE	c	RMSE
1.5	2.387	1.326(-07)	1.651	1.679(-06)
2	1.322	6.747(-09)	1.238	1.227(-08)
2.5	1.727	4.820(-10)	0.991	2.181(-09)
3	1.260	5.952(-10)	0.826	9.546(-09)
3.5	1.177	2.509(-09)	0.708	2.899(-09)
4	1.309	1.004(-08)	0.619	7.294(-09)
4.5	0.814	6.669(-09)	0.550	1.706(-08)

Example 5 We finally consider the Kirchhoff thin plate problem [28]:

$$\Delta^2 u(x,y) = \frac{q}{D}, \quad (x,y) \in \Omega, \tag{41}$$

$$u(x,y) = 0, \quad (x,y) \in \partial\Omega, \tag{42}$$

$$\frac{\partial}{\partial n} u(x,y) = 0, \quad (x,y) \in \partial\Omega, \tag{43}$$

where Ω is a polygonal domain, $u(x, y)$ is the deflection of the plate, $q = 10^6$ is the constant transverse load, $D = Eh^3/(12(1-\mu^2))$ is the flexural rigidity, $E = 2.1 \times 10^{11}$ is the elastic modulus of steel, $h = 0.01$ is the thickness of the plate, and $\mu = 0.3$ is Poisson's ratio for steel.

In the numerical implementation, we took $N_i = 463$, $N_b = 135$, and the radius of the ghost circle to be $R = 2.2$. In Figure 12, we show the profile of the polygonal domain and the distribution of the interior points (green •), boundary points (blue •), ghost points (red •), and source points (black •). In this example we placed the source points on a fictitious boundary which is similar in shape to the boundary $\partial\Omega$. More specifically, the location of the source point (x_s, y_s) corresponding to the boundary point (x_b, y_b) is given from

$$(x_s, y_s) = (x_b, y_b) + d\,(n_x, n_y), \tag{44}$$

where (n_x, n_y) is the unit normal vector to the boundary at (x_b, y_b) and d determines the distance between the boundary points and their corresponding source points. Alternatively, the source points may be placed on a circle in the previous examples. However, in this case, the accuracy is very sensitive to the radius of the source circle $\mathcal{R}$. Extensive experimentation indicated that $\mathcal{R}$ should be chosen close to 1. Consequently, we decided to use the source location obtained from (44) and shown in Figure 12. For the selection of the MQ shape parameter, we found that the modified Franke formula produced satisfactory results.

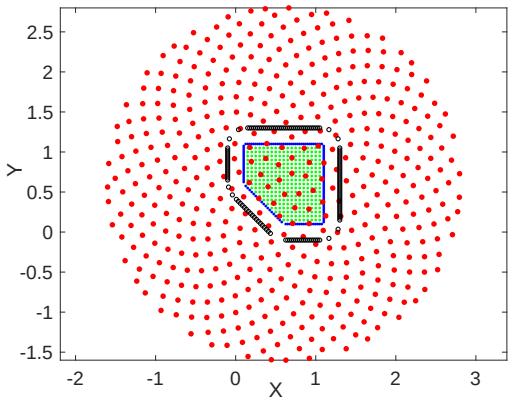

Figure 12: Example 5: The profiles of interior points (green •), boundary points (blue •), ghost points (red •), and source points (black •).

Since no exact solution is available for this problem, we compared our results with those in [28] where trigonometric basis functions were employed. Figure 13(a) shows the profile of the approximate solution while the corresponding absolute error plot obtained

with $d = 0.3$ in (44) is presented in Figure 13(b). The overall RMSE is $6.370(-6)$. The results in Table 6 indicate that the source points should be neither too close nor too far away from the boundary. This is in sharp contrast to the previous four examples where the accuracy appeared to be insensitive to the source location.

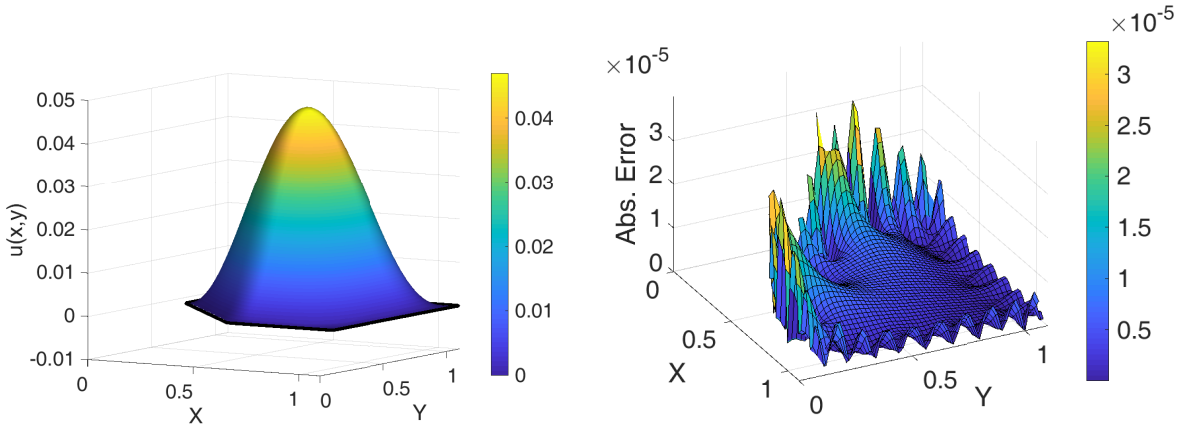

(a) (b)

Figure 13: Example 5. The profiles of (a) the approximate solution and (b) the absolute error.

Table 6: Example 5: The errors between the results obtained with the current method and those in [28] using various source locations with fixed ghost circle radius $R = 2.2$.

d	RMSE
0.1	1.150(-02)
0.2	6.779(-06)
0.4	5.543(-06)
0.6	7.739(-06)
0.8	4.704(-05)
1.0	7.185(-05)

To investigate the impact of the ghost circle radius R, we fixed the source points with $d = 0.2$ and computed the RMSE errors for various R. Figure 14(a) shows that the size of the ghost circle has little impact on the accuracy. The results presented in Table 6 and Figure 14 demonstrate that the proposed method is fairly stable and accurate even in the case when the exact solution is not available. In Figure 14(b), we show the accuracy with respect to the shape parameter c using $R = 2.4, d = 0.3$. From this figure, we observe that the accuracy is insensitive to the values of the RBF shape parameter. As

identifying a good RBF shape parameter is not an easy task, this observation indicates that the proposed method has the advantage of being numerically stable.

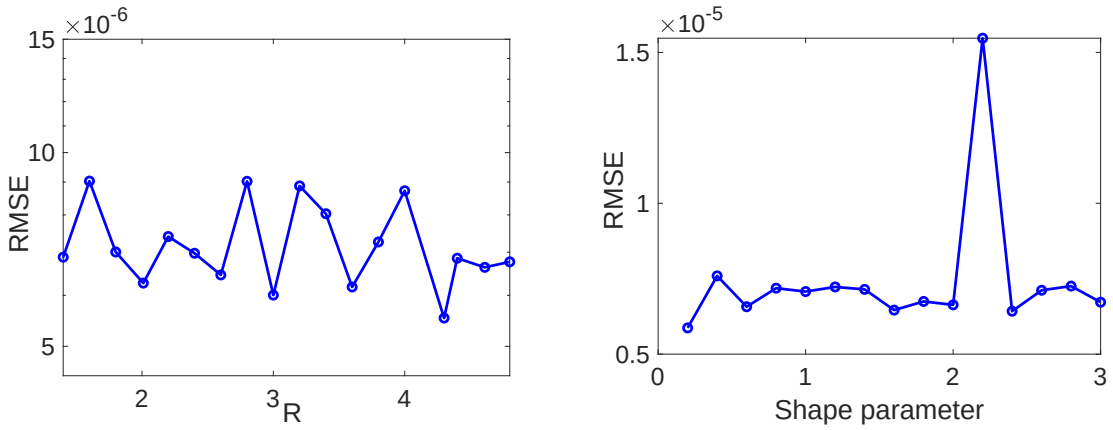

(a) (b)

Figure 14: Example 5: (a) The accuracy for various radii R using $d = 0.3$. (b) RMSE versus shape parameters using $R = 2.4, d = 0.3$.

7 Conclusions

In this paper, we propose a novel application of the fictitious points method in which the centres of the RBFs are distributed inside and outside the domain of the BVP in question in the context of the one–step MPS–MFS. An important issue in the implementation of RBF methods is how to choose the shape parameter in order to achieve optimal accuracy. To address this, we use the modified Franke formula as a predictor for an initial estimate of the shape parameter and then employ LOOCV as a corrector for the selection of an appropriate shape parameter in the MQ–RBF method. In addition to the choice of an appropriate value of the shape parameter, the selection of the RBF fictitious points (that is, the size of the circle/sphere in which they are distributed) is also crucial for obtaining good accuracy. In contrast, the accuracy of the method is less sensitive to the selection of the MFS source points in the inhomogeneous equation cases studied. Their placement on a fictitious source circle/sphere appears to be adequate for most 2D/3D problems considered. This was not true, however, for Example 5 where a fictitious boundary similar in shape to the problem boundary had to be used. It is noteworthy that this is the first time the MPS and the MFS are combined with their own respective fictitious points. The efficacy and accuracy of the proposed method are demonstrated by considering five numerical examples in 2D/3D and second/fourth–order PDEs

with variable coefficients and in highly irregular domains. Another attractive feature of the proposed method is its simplicity and that fact that the whole solution procedure is truly meshless. Its extension to time–dependent and nonlinear problems is currently under investigation.

Acknowledgement

The second author acknowledges the support of the National Natural Science Foundation of China (No. 11501086) and the Fundamental Research Funds for the Central Universities (No. ZYGX2016J137).

References

[1] K. E. Atkinson, *The numerical evaluation of particular solutions for Poisson's equation*, IMA Journal of Numerical Analysis, **5**, 319-338, 1985.

[2] K. Balakrishnan and P. A. Ramachandran, *Osculatory interpolation in the method of fundamental solution for nonlinear Poisson problems*, Journal of Computational Physics, **172**, 1–18, 2001.

[3] C. S. Chen, C. M. Fan and J. Monroe, *The method of fundamental solutions for solving elliptic partial differential equations with variable coefficients*, in The Method of Fundamental Solutions - A Meshless Method, eds. C. S. Chen, A. Karageorghis and Y. S. Smyrlis, Dynamic Publishers, Inc., Atlanta, pp. 75–105, 2008.

[4] C. S. Chen, A. Karageorghis and Y. Li, *On choosing the location of the sources in the MFS*, Numerical Algorithms, **72**, 107–130, 2016.

[5] C. S. Chen, A. Karageorghis and F. Dou, *A novel RBF collocation method using fictitious centres*, Applied Mathematics Letters, **101**, 106069, 2020.

[6] G. Fairweather and A. Karageorghis, *The method of fundamental solutions for elliptic boundary value problems*, Advances in Computational Mathematics, **9**, 69–95, 1998.

[7] G. Fairweather, A. Karageorghis and P. A. Martin, The method of fundamental solutions for scattering and radiation problems, Engineering Analysis with Boundary Elements, **27**, 759–769, 2003.

[8] C. M. Fan, C. S. Chen and J. Monroe, The method of fundamental solutions for solving convection–diffusion equations with variable coefficients, Advances in Applied Mathematics and Mechanics, **1**, 215–230, 2009.

[9] G. E. Fasshauer and J. G. Zhang, *On choosing optimal shape parameters for RBF approximation*, Numerical Algorithms, **45**, 345–368, 2007.

[10] A. I. Fedoseyev, M. J. Friedman and E.J. Kansa, *Improved multiquadric method for elliptic partial differential equations via PDE collocation on the boundary*, Computers and Mathematics with Applications, **43**, 439–455, 2002.

[11] B. Fornberg, A pseudospectral fictitious point method for high order initial-boundary value problems, SIAM Journal on Scientific Computing, **28**, 1716–1729, 2006.

[12] R. Franke, *Scattered data interpolation: tests of some methods*, Mathematics of Computation, **38**, 181–200, 1982.

[13] M. A. Golberg, C. S. Chen and S. R. Karur, *Improved multiquadric interpolation for partial differential equations*, Engineering Analysis with Boundary Elements, **18**, 9–17, 1996.

[14] M. A. Golberg and C. S. Chen, *The method of fundamental solutions for potential, Helmholtz and diffusion problems*, Boundary Integral Methods: Numerical and Mathematical Aspects (M. A. Golberg, ed.), Comput. Eng., vol. 1, WIT Press/Comput. Mech. Publ., Boston, MA, 1999, pp. 103–176.

[15] W. Hui and Q. Qinghua, *Some problems with the method of fundamental solution using radial basis functions*, Acta Mechanics Solida Sinica, **20**, 21–29, 2007.

[16] A. Karageorghis and G. Fairweather, *The method of fundamental solutions for the numerical solution of the biharmonic equation*, Journal of Computational Physics, **69**, 434–459, 1987.

[17] L. H. Kuo, *On the selection of a good shape parameter for RBF approximation and its applications for solving PDEs*, Ph.D. Dissertation, University of Southern Mississippi, 2015.

[18] V. D. Kupradze and M. A. Aleksidze, *The method of functional equations for the approximate solution of certain boundary value problems*, U.S.S.R. Computational Mathematics and Mathematical Physics, **4**, 82–126, 1964.

[19] E. Larsson and B. Fornberg, *A numerical study of some radial basis function based solution method for elliptic PDEs*, Computers and Mathematics with Applications, **46**, 891–902, 2003.

[20] R. Mathon and R. L. Johnston, *The approximate solution of elliptic boundary value problems by fundamental solutions*, SIAM Journal on Numerical Analysis, **14**, 638–650, 1977.

[21] J. Monroe, *Hybrid meshless method for numerical solution of partial differential equations*, University of Southern Mississippi, Ph.D. Dissertation, 2014.

[22] S. Rippa, *An algorithm for selecting a good value for the parameter c in radial basis function interpolation*, Advances in Computational Mathematics, **11**, 193–210, 1999.

[23] A. Safdari–Vaighani and E. Larsson, *Radial basis function methods for the Rosenau equation and other higher order PDEs*, Journal of Scientific Computing, **75**, 1555-1580, 2018.

[24] R. Schaback, *Adaptive numerical solution of MFS systems*, in The Method of Fundamental Solutions – A Meshless Method, eds. C. S. Chen, A. Karageorghis and Y. S. Smyrlis, Dynamic Publishers, Inc., Atlanta, 2008, pp. 1–27.

[25] T. Shigeta, D. L. Young and C. S. Liu, *Adaptive multilayer method of fundamental solutions using a weighted greedy QR decomposition for the Laplace equation*, Journal of Computational Physics, **231**, 118–7132, 2012.

[26] H. Vogel, *A better way to construct the sunflower head*, Mathematical Biosciences, **44**, 179–189, 1979.

[27] H. Wang and Q. H. Qin, *A meshless method for generalized linear or nonlinear Poisson-type problems*, Engineering Analysis with Boundary Elements, **30**, 515–521, 2006.

[28] D. Wang, C. S. Chen and W. Li, *An efficient MAPS for solving fourth order partial differential equations using trigonometric functions*, Computers and Mathematics with Applications, `https://doi.org/10.1016/j.camwa.2019.08.005`

[29] The Stanford 3D Scanning Repository, Stanford Computer Graphics Laboratory, `http://graphics.stanford.edu/data/3Dscanrep/`.

[30] `http://www.math.usm.edu/cschen/3D-gear/`